Available online at www.sciencedirect.com
ScienceDirect
Journal of the European Ceramic Society 31 (2011) 2167–2174
www.elsevier.com/locate/jeurceramsoc

Resistance to oxidation of graphite silicided by reactive infiltration

Rana Israel [a,b], Guillaume de Combarieu [c], Béatrice Drevet [a,*], Denis Camel [a], Nicolas Eustathopoulos [b], Olivier Raymond [c]

[a] CEA/LITEN, INES, Savoie-Technolac, BP 332, 50 av. Lac Leman, 73377 Le-Bourget-du-Lac, France
[b] SIMAP/Grenoble-INP, Domaine Universitaire, 38402 St Martin d'Hères, France
[c] MERSEN France, 41 rue Jean Jaurès, 92231 Gennevilliers, France

Received 23 December 2010; received in revised form 18 April 2011; accepted 5 May 2011
Available online 1 June 2011

Abstract

In order to improve the oxidation resistance of graphite at high temperatures, graphite surfaces are modified by two silicidation processes involving reactive infiltration of molten silicon or, alternatively, of gaseous silicon monoxide.

The resistance to oxidation of silicided graphite is studied by cyclic oxidation tests performed under a dry air flux at temperatures in the range 1550–1600 °C.

During oxidation three successive regimes are evidenced: (i) initial growth of a passive silica layer on the continuous SiC superficial layer responsible for the remarkable oxidation resistance at 1550 °C; (ii) then, slow mass consumption in the intermediate composite SiC–C region; (iii) and finally, rapid local consumption of the underlying non-infiltrated porous graphite.

The temporal stability of the silicided layer in air is analyzed and the reactions affecting this stability are identified. The analysis interprets the experimental findings in a satisfactory manner, especially the dramatical variation with temperature of silicided graphite lifetime observed in this temperature range.

Keywords: D. Carbon; D. SiC; C. Corrosion; C. Lifetime; Infiltration

1. Introduction

For the preparation of photovoltaic (PV) silicon from the melt, graphite is widely used as a high temperature material for structural parts, thermal insulation, and even crucibles. Interaction of these parts with the reactive atmosphere is a main cause of graphite degradation limiting the lifetime of this material. Especially severe are the conditions imposed during Si purification by the metallurgical route[1] including two purification steps performed under oxidizing atmospheres at temperatures as high as 1550–1600 °C. Due to its very weak resistance to oxidation, unprotected graphite can hardly be used as crucible material in these operations. For instance, unprotected graphite in contact with oxidizing atmospheres at temperatures of 800–1000 °C for 1 h exhibits mass losses of 20–50% depending on graphite microstructure and temperature.[2,3]

In order to increase the crucible lifetime, a surface treatment is needed to form a dense non-reactive protective layer on the porous graphite. Specific requirements for PV applications are that the protective layer be pure to avoid Si pollution by electrically active impurities, and that the process be cheap and can be applied to large dimensions.

Numerous studies have been devoted to graphite protection by silicon carbide layers and promising results have been obtained.[2,4,5] However, the treatments used in these studies are complex, involving formation of several sub-layers (including CVD layers), and it therefore becomes difficult to use them for PV Si preparation. Of particular interest is the study by Chunhe and Jie,[3] where a relatively simple, one-step treatment was used, consisting of reactive infiltration of molten silicon. A further advantage of such a treatment is that it avoids, at least in its principle, any additional source of pollution. However, the maximum temperature investigated by these authors in

* Corresponding author. Tel.: +33 4 79 44 45 95; fax: +33 4 79 62 37 71.
E-mail address: beatrice.drevet@cea.fr (B. Drevet).

0955-2219/$ – see front matter © 2011 Elsevier Ltd. All rights reserved.
doi:10.1016/j.jeurceramsoc.2011.05.005

their oxidation tests was 1500 °C, i.e. lower than the temperature range of 1550–1600 °C explored in the present study. It must be emphasized that, as found previously with different types of silicon carbide, several SiC degradation processes (reviewed in [6]) come into play at temperatures higher than but close to 1500 °C (see also Section 4).

In the present investigation, reactive silicidation of graphite by liquid Si (denoted in the following as RLI) is performed on the basis of a previous study of the mechanisms of capillary interactions between porous graphite and molten silicon.[7,8] Alternatively, silicidation is also produced for the same type of graphite by reactive gaseous infiltration (denoted as RGI) of a silicon-carrying molecule (SiO).[5,9] The resistance to oxidation of silicided graphite at 1550–1600 °C is characterized at the laboratory scale by cyclic oxidation tests. As will be shown later, at these high temperatures, the microstructure of the silicided zone is of crucial importance for the resistance to oxidation. For this reason, emphasis is placed on the characterization of the initial microstructure of the protective surface layer and its change during oxidation. Although both optical and scanning electron microscopy (SEM) have been used, in most cases optical images were preferred as they provide a better contrast of silicided graphite constituents than images obtained by SEM.

2. Experimental procedure

The type of graphite was first selected on the basis of the previous study of liquid Si/graphite interaction mechanisms.[7,8] The study showed that the infiltration of liquid Si into porous graphite is promoted by the reaction of formation of SiC on the pore walls at the infiltration front:

$$\mathrm{Si(l)} + \mathrm{C(s)} \rightarrow \mathrm{SiC(s)} \quad (1)$$

During infiltration, the reaction (1) continues behind the infiltration front and leads ultimately to pore closure at the sample entrance and to infiltration interruption. The size and microstructure of the infiltrated zone depends on process parameters (time and temperature) and on graphite microstructure, which is characterized by its porosity, pore size distribution and average pore diameter. In particular, a small pore size is required to ensure full conversion of the infiltrated silicon into SiC, but if the pores are too small this leads to premature pore closure and thus to small infiltration depths. The maximum value of SiC volume fraction α_{SiC} that can be reached in the infiltration area is proportional to pore volume fraction α_p ($\alpha_{SiC} = 1.786\alpha_p$ [10]). Therefore, to obtain a high conversion rate of carbon to silicon carbide, high-porosity graphite should be used. However, if the porosity is too high, this may lead to crack formation and even to graphite fracture due to stresses generated by the reaction during infiltration.[7] Finally, taking into account the additional requirement to be able to manufacture large parts at reasonable cost, graphite 2020PT of Mersen (Gennevilliers, France), with the properties summarized in Table 1, was selected. A further advantage of this type of graphite is its expansion coefficient value, close to the expansion coefficient of silicon carbide ($5.7 \times 10^{-6}\,K^{-1}$ at 1000 °C [11]), which allows the thermal stresses generated during cooling to be minimized.

The silicidation by liquid Si infiltration consists of dipping graphite parallelepipeds of 2 cm × 2 cm × 1 cm into the Si melt contained in a crucible of diameter 5 cm made of glassy carbon. In order to hold the piece while ensuring that it will finally be fully protected by SiC, it is previously brazed to a graphite rod by a specific process described elsewhere.[12] The retained immersion parameters are 2 h at 1500 °C. This immersion duration is much longer than the time at which infiltration stops (less than 10 min). This is in order to ensure that all the infiltrated silicon is consumed by reaction (1).

The silicidation by reactive gaseous infiltration consists of immersing the graphite part into a powder mixture of SiO_2 and SiC and heating at high temperature (close to 1800 °C) under a flow of argon. The reaction between silica and silicon carbide leads to the formation of gaseous silicon monoxide according to[5,13]:

$$2\mathrm{SiO_2(s)} + \mathrm{SiC(s)} \rightarrow 3\mathrm{SiO(g)} + \mathrm{CO(g)} \quad (2)$$

The SiO(g) then diffuses into interconnected graphite porosity and reacts with C forming SiC:

$$2\mathrm{C(s)} + \mathrm{SiO(g)} \rightarrow \mathrm{SiC(s)} + \mathrm{CO(g)} \quad (3)$$

The mechanisms of this reaction were discussed in [14]. The method is first applied to 2 cm × 2 cm × 1 cm samples, then to crucibles of 50 mm diameter.

The oxidation of silicided graphite is studied by placing the samples in the isothermal zone of a tubular alumina chamber furnace of 70 mm internal diameter, heating to the test temperature and then exposing them to a flow of dry air (less than 3 ppm water) at a rate of 0.5 l/min for given durations in successive cycles. Between each cycle, the sample is cooled and weighed with a microelectronic balance with an accuracy of 0.5 mg, and its surface is examined by optical microscopy. After the final cycle, several metallographic sections are made to examine the general aspect of the reaction layer and the particular defects which may have appeared.

3. Results

The microstructure obtained after silicidation by liquid Si is the result of the reactive infiltration process analyzed in detail in [7]. It consists of two well defined regions (Fig. 1): (i) a continuous SiC surface layer resulting from the reaction between the graphite surface and the bulk liquid, and (ii) a composite graphite–SiC region resulting from the reactive infiltration of liquid Si. The average thickness of the surface layer is 15 μm with minimum and maximum values equal to 5 and 25 μm respectively. The depth of the composite zone is close to 700 μm. Neither the thickness of the surface layer nor that of the infiltrated zone can be increased by increasing the holding time at 1500 °C (up to 6 h), or the temperature (up to 1600 °C).[15] Note that, in relation with the duration of the applied treatment, the infiltrated zone no longer contains residual silicon, and that the surface layer appears homogeneous and formed by crystals the

Table 1
Properties of the graphite used in the present study (2020PT of Mersen).

Density (g cm^{-3})	Porosity (%)	Average pore diameter (μm)	Expansion coefficient (K^{-1})	Flexural strength (MPa)	Compressive strength (MPa)
1.77	15	2.3	4.5×10^{-6}	45	99

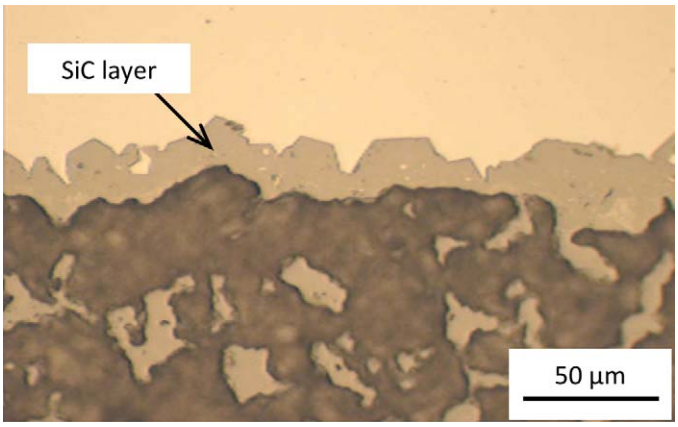

Fig. 1. Microstructure of graphite silicided by RLI. Optical image.

size of which is of the order of the thickness of the layer. In the composite region, graphite remains largely the majority phase; indeed, for $\alpha_p = 0.15$, the maximum SiC fraction which can be reached if all pores of the graphite are filled is $\alpha_{SiC} = 0.26$.

An example of the microstructures obtained after RGI is shown in Fig. 2. Here the depth of infiltration is in the mm range. SiC appears as the majority phase in the region close to the graphite surface, and its fraction progressively decreases with increasing depth. Note that the maximum SiC fraction α_{SiC} which can be reached by carbon conversion through reaction (3) is now given by $\alpha_{SiC} = 8.33\alpha_p$.[16] The factor 8.33 is well above the proportionality factor 1.786 between α_{SiC} and α_p in the case of the reaction (1). This is due to the fact that the formation of one mole of SiC by the reaction (3) needs the consumption of two moles of carbon against only one by the reaction (1). According to the equation $\alpha_{SiC} = 8.33\alpha_p$, the minimum value of pore fraction for obtaining a layer consisting only of SiC is 0.12 which is slightly lower than the porosity of 2020PT graphite used in the present study. Nevertheless, some large dense graphite grains, which were present in the initial graphite microstructure, remain unconverted. Due to the high conversion ratio into SiC in the upper region, these grains are isolated by the SiC matrix, and thus not directly connected to the underlying graphite. Due to the presence of these grains near the surface, the continuous superficial SiC layer is of irregular thickness, ranging from 20 to 100 μm. Fig. 2 also shows the presence in this layer of small, micron-sized, non-reacted graphite particles, as well as several micron-sized particles, identified by EDXS as free silicon. Si micro-droplets result from the reaction:

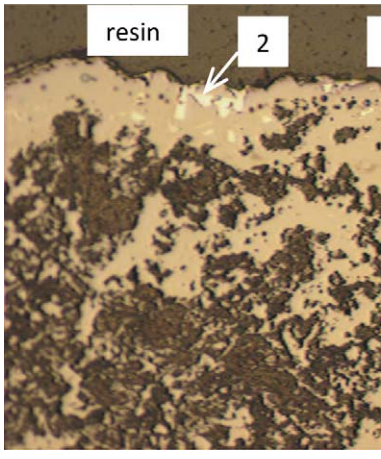

Fig. 2. Microstructure of graphite silicided by RGI. The arrows 1 and 2 show graphite and free silicon particles respectively lying in the continuous SiC layer.

Table 2
Mass variation of graphite silicided by RGI during successive oxidation cycles at 1550 °C for a parallelepiped with initial mass $m = 7.8348$ g (sample PP1 in Fig. 3).

Cycle	Duration (h)	Δm (mg)	Δm (%)
1	3	+6.5	+0.083
2	14	+11.6	+0.148
3	14	−0.9	−0.011
4	26	−15.9	−0.200
5	17	−20	−0.255

$$SiC(s) + SiO(g) \rightarrow 2Si(l) + CO(g) \quad (4)$$

which accompanies the main reaction (3) during infiltration of SiO(g).

Table 2 gives the mass variation measured between successive oxidation cycles at 1550 °C for a graphite parallelepiped silicided by RGI. Fig. 3 presents the cumulated variation of sample mass *per unit area* as a function of total oxidation time for this experiment. By this representation, it is possible to compare

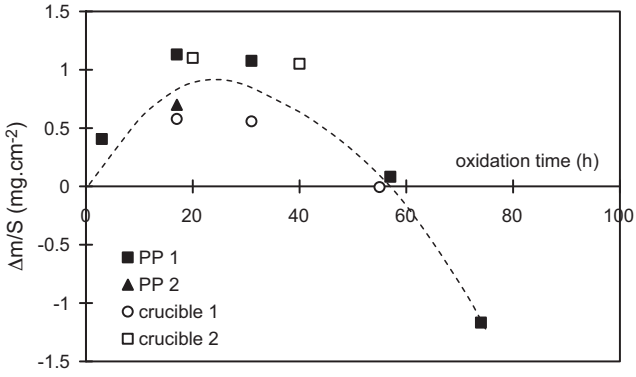

Fig. 3. Total mass variation per unit surface area of graphite silicided by RGI during successive oxidation cycles at 1550 °C for both parallelepipedic samples (noted PP) and crucibles.

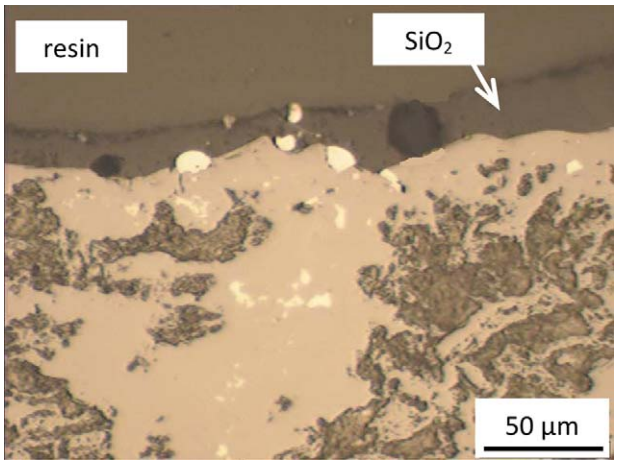

Fig. 4. Silica scale containing bubbles on the surface of graphite silicided by RGI after an oxidation treatment of 74 h at 1550 °C.

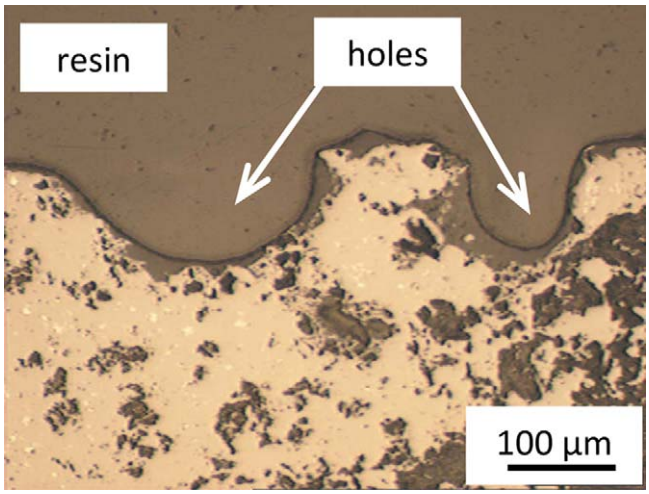

Fig. 5. Part of graphite silicided by RGI containing holes. The holes correspond to burnt graphite particles after an oxidation treatment of 74 h at 1550 °C.

the results obtained on samples with different masses and shapes (parallelepipeds, denoted as PP, and crucibles). Fig. 3 shows that these factors do not affect the results. This clearly indicates that oxidation is not controlled by oxygen transport in the gas but by a process taking place in the passive layer (see the next section). Fig. 3 shows that the sample mass first increases with time, then starts to decrease and after about 55 h becomes lower than its initial value.

The surface of the sample PP1, concerned by the results of Table 2, presented after the fifth cycle some localized defects consisting of cavities with a diameter ranging from a few tens to a few hundreds of microns. The sample surface seems to be covered by a silica layer revealed by the glassy external appearance of the samples. This is clearly evidenced on the metallographic cross-section performed on a part without defects (Fig. 4). As can be seen in this figure, the silica layer contains bubbles.

The silica layer is obviously formed by passive oxidation of SiC:

$$2SiC(s) + 3O_2(g) \rightarrow 2SiO_2(s) + 2CO(g) \quad (5)$$

The formation of a silica layer a few tens of microns thick is responsible for the increase in sample mass during the first 20 h of oxidation (the consumption of one mole of SiC by the reaction (5) leads to a mass gain of 18 g).

Fig. 5 shows a part of the sample containing cavities. Theses cavities are located in the infiltrated zone and correspond to graphite particles burnt by the reaction with air. The graphite combustion in the dense graphite + SiC composite region contributes to the mass losses of the sample found at $t > 30$ h (Table 2 and Fig. 3). However, even after 74 h at 1550 °C, the total mass losses remain small (of the order of 1%) because, at this time, the oxidation front has not yet reached the non-infiltrated porous graphite region although it was close to it.

Much more rapid mass loss starts when the non-infiltrated zone is locally reached. There, the porous graphite begins to be consumed by a 3D reaction process, which is much faster than the 2D process occurring in the non-porous composite region above. This stage was evidenced by experiments performed at 1600 °C. While after a first oxidation cycle of 5 h at this temperature, the mass loss was very small (close to 0.2%), after a second cycle of 20 h it attained 10%. Examination of the sample shows the presence of several wells at the surface which communicate with large cavities in the underlying graphite (Fig. 6). The lifetime of graphite silicided by RGI or RLI is defined as the time after which this third stage of rapid mass loss starts.

Further experiments were carried out with graphite silicided by RLI. After 45 h at 1550 °C, a millimeter sized hole appeared on a face of the sample. Fig. 7 shows a metallographic section of the sample passing through the hole. It can be seen that the material has not been attacked uniformly but starting at two points on the surface. The attack has first created a well in the infiltrated zone and then attained the non-infiltrated, porous graphite. The attack was likely initiated at areas where the thickness of the continuous SiC superficial layer is very small. Indeed, as noted above, while the average thickness of this layer is 15 µm for RLI-graphite, at some points it can be as low as 5 µm (Fig. 1) (similar variations between the average and minimum thicknesses are also found for the continuous SiC layer formed on

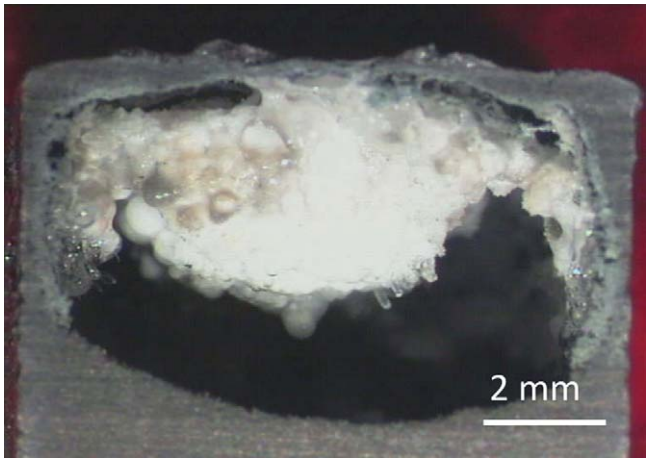

Fig. 6. Metallographic cross-section of a PP sample silicided by RGI after an oxidation treatment of 20 h at 1600 °C showing a region lying below a well appearing on the sample surface (see text).

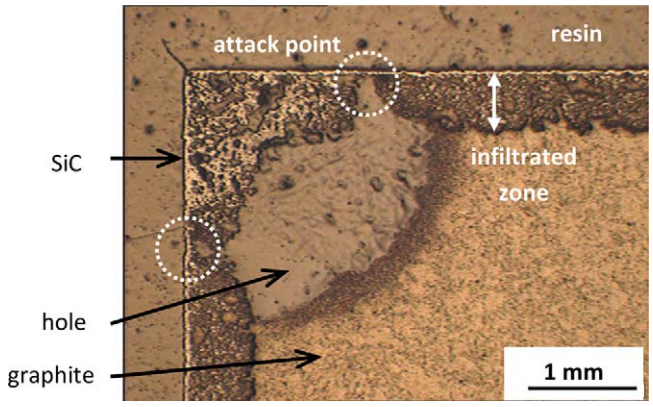

Fig. 7. Metallographic cross-section of a PP sample silicided by RLI after an oxidation treatment of 45 h at 1550 °C showing a region of localized attack.

RGI-graphite, see above). A second experiment performed at the same temperature (1550 °C), time (45 h) and number of cycles (4), confirmed the result of the first experiment, namely sample attack down to depths of several hundred microns, with the oxidation front arriving quite close to the non-infiltrated region (Fig. 8a). Therefore, the lifetime of this sample was very close to 45 h. Fig. 8b and c shows the surface of the sample at points 1 and 2. At point 2, the SiC layer is still present on the outer surface while at point 1 this layer is no longer present and oxidation at this point affects directly the composite graphite-SiC zone.

From the above results, it can be concluded that oxidation at 1550 °C in air of graphite silicided by RGI or RLI takes place in three different stages: initial growth of a passive silica layer formed on the continuous SiC superficial layer leading to an increase in sample mass, followed by a slow mass loss corresponding to oxidation of the intermediate composite SiC–C region and finally, rapid mass loss due to active oxidation of the underlying non-infiltrated porous graphite.

Table 3 summarizes the results of tests for both parallelepipeds and crucibles. Silicidation by RGI leads to superior results because the thickness of the continuous SiC superficial layer is higher by a factor 5–6 for RGI-graphite than for RLI samples.

4. Discussion

The results of oxidation tests show an initial increase in sample mass at 1550 °C (Fig. 3). Similar increases were observed at 1500 °C and 1350 °C.[17] These results do not agree with those obtained by Chunhe and Jie[3] with RLI graphite, who found that after 2 h in air at 1500 °C, the mass loss was 1%, which is nearly the same as the mass loss observed for the same time at a much

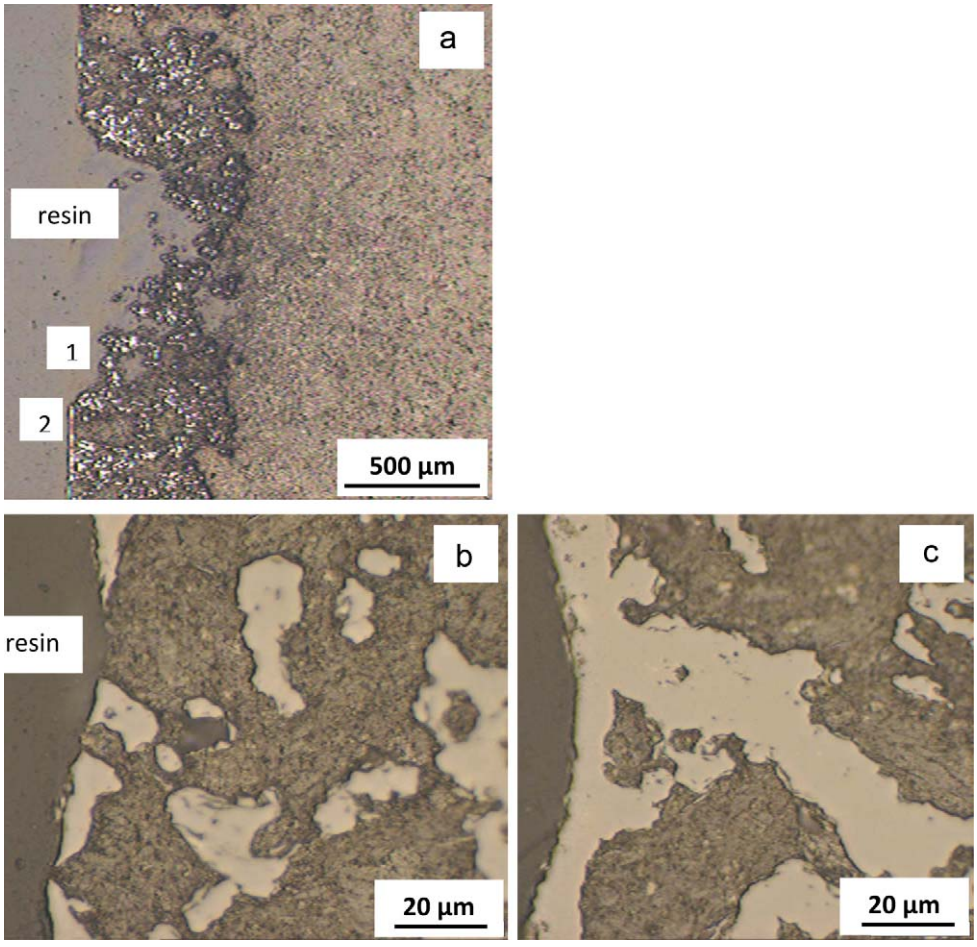

Fig. 8. Metallographic cross-section of a PP sample silicided by RLI after an oxidation treatment of 45 h at 1550 °C showing a region of localized attack. (a) Overall view. (b, c) Magnifications of regions 1 and 2 respectively.

Table 3
Lifetime for different types of silicidation and different shapes of graphite samples. The lifetime is taken as the time needed for oxidation to reach the non-infiltrated porous graphite core.

Sample shape	Silicidation	Oxidation temperature (°C)	Number of cycles	Lifetime (h)
PP	RLI	1550	4	31–45
PP	RLI	1550	4	45
PP	RGI	1550	5	74
PP	RGI	1600	2	5
Crucible	RGI	1550	3	>55
Crucible	RGI	1550	2	>40

PP: parallelepiped of 2 cm × 2 cm × 1 cm; crucible: diameter 5 cm; RLI: reactive liquid infiltration; RGI: reactive gaseous infiltration.

lower temperature (1000 °C). However in the experiments of these authors, mass loss was observed from the beginning of the oxidation test, i.e. the increasing branch of the $\Delta m/S$ vs time curve of Fig. 3 is missing. This result strongly suggests the presence, in the superficial SiC layer of their samples, of defects allowing direct contact between oxygen and the underlying graphite particles.

As noted in the previous section, the initial increase in sample mass is due to the growth of a passive silica layer (reaction (5)). It is generally accepted[6] that at temperatures higher than 1350 °C, silica growth is limited by the diffusion of oxygen ions in the passive layer towards the SiO_2/SiC interface. Moreover, the parabolic constant k_p relating the layer thickness e to time t ($e^2 = k_p t$) is nearly independent of the oxygen partial pressure. The value of k_p that can be deduced from data of Fig. 3 for $t \leq 25$ h is 2×10^{-15} m^2/s. This is within the literature values obtained for various types of SiC (sintered, CVD, monocrystalline) at temperatures higher than 1350 °C, lying between 5×10^{-17} m^2/s and 10^{-14} m^2/s.[6] Note that our value is close to the upper limit of values given in the literature. It is possible that the growth rate of silica on RGI samples is enhanced by the presence of silicon micro-droplets (note that silicon oxidation also leads to the formation of silica, just like oxidation of SiC).

The maximum observed on the $\Delta m(t)/S$ curve (Fig. 3) indicates the occurrence of one or more processes acting to decrease the sample mass. Such a mass loss can be produced by *silica volatilization*[6,18] resulting from the reactions:

$$SiO_2(s) \rightarrow SiO_2(g) \quad (6a)$$

$$SiO_2(s) \rightarrow SiO(g) + \frac{1}{2}O_2(g) \quad (6b)$$

Using thermodynamic data of,[19] it can readily be seen that at 1550 °C and in air the predominant species in the gas is silica vapour with a partial pressure $P_{SiO_2} = 1.5 \times 10^{-8}$ atm. Then, the erosion rate of silica can be calculated using the expression:

$$\frac{de}{dt} = -\frac{V_m D_{SiO_2} P_{SiO_2}}{RT\delta} \quad (7)$$

where V_m is the molar volume of silica (27.27 cm^3), D_{SiO_2} is the diffusion coefficient of gaseous silica in air (≈3 cm^2 s^{-1} [13]), T is the temperature in Kelvin and δ is the thickness of the diffusion boundary layer in the gas. The value of δ, depending mainly on sample geometry and on gas flow rate, was estimated by the method described in [20] and found to lie between 4.3 mm for a spherical sample and 55 mm for a plate. Using these values of δ, the thickness of silica evaporated in 100 h, calculated with Eq. (7), takes negligible values lying between 2 and 30 nm. As shown in [21–23], silica evaporation becomes an effective mechanism accounting for significant mass losses at temperatures close to 1550 °C only in low P_{O_2} environments. In air, much higher temperatures, more than 1800 °C, are needed.

Another process that can explain the mass losses observed at times greater than 30 h (Fig. 3) is the *reduction of the silica scale by the underlying SiC* occurring at the SiO_2/SiC interface according to reaction (2). In view of the presence of graphite particles in the SiC continuous layer, it is assumed that the SiC in this layer is saturated in carbon, i.e. that SiC is in equilibrium with graphite. This condition is taken into account by considering that reaction (2) is accompanied by the reaction (8a):

$$C(s) + SiO_2(s) \rightarrow SiO(g) + CO(g) \quad (8a)$$

For a system including the gas phase and three condensed phases (silicon carbide, graphite and silica) the thermodynamic variance is equal to unity. Therefore, the equilibrium partial pressures of SiO and CO species depend only on temperature. Using data of[19] it was found that the condition

$$P_{SiO} + P_{CO} = 1 \text{ atm} \quad (9)$$

is satisfied at 1525 °C. Therefore, for our experiments, performed under a total pressure of 1 atm, 1525 °C is the minimum temperature for bubble formation. This calculation result is compatible with bubbles observed in the scale at 1550 °C (Fig. 4).

It must be emphasized that at 1550 °C neither the reaction (2) alone (giving a total pressure of 0.05 atm calculated taking $P_{SiO} = 3P_{CO}$), nor the reaction (8a) alone (total pressure of 0.20 atm calculated taking $P_{SiO} = P_{CO}$) can account for bubble formation. Only the reaction (2) with carbon-saturated SiC is able to do this.

Given the presence of Si micro-droplets in the continuous SiC layer, the hypothesis of a SiC locally saturated in silicon was checked. This implies that the reaction (2) would not be accompanied by (8a) but, alternatively, by reaction (8b):

$$Si(l) + SiO_2(s) \rightarrow 2SiO(g) \quad (8b)$$

However, the temperature at which the sum of calculated SiO and CO pressures becomes equal to 1 atm is 1840 °C, which

is much higher than the experimental temperature of 1550 °C. Thus, only the reaction (2) accompanied by the reaction (8a) can account for the experimental observations. Bubbles have also been observed in previous studies of oxidation of CVD SiC coatings[22,24] and explained by assuming that the SiC in CVD coatings is saturated in carbon.[24]

From the above discussion, it is concluded that the behaviour of silicided graphite in air at 1550 °C is dictated by the competition of two reactions occurring at the silica/silicon carbide interface. (i) The first is silica growth taking place by reaction between SiC and oxygen. The rate of this reaction, limited by the diffusion of oxygen ions in the scale, decreases rapidly with time due to the increasing thickness of the scale (for diffusion-limited growth de/dt varies as $e(t)^{-1}$). (ii) The second reaction is silica consumption by reaction between the scale and silicon carbide saturated in carbon. For short times (small e values), the growth reaction predominates, as shown by the initial mass gain of the material, while for long experimental times the silica consumption reaction predominates, as testified by sample mass losses and by bubble formation.

The above description applies to passive oxidation of SiC saturated in carbon. In our samples, saturation is attested by the presence, in the continuous SiC layer, of graphite particles which can attain, in some cases, a size of several tens of microns and even more. These particles have a second effect on the oxidation behaviour in as much that bubble disruption can provoke direct contact between these particles and air, thus leading to their rapid consumption and to further mass losses (Fig. 5). However, as long as graphite grains are isolated in a SiC matrix, these losses remain limited. The mass losses increase when the reaction front reaches the composite region consisting of SiC and interconnected graphite grains (2D oxidation). Finally, when the reaction front reaches the non-infiltrated porous graphite, the sample mass decreases very rapidly due to the oxidation of interconnected graphite grains by a 3D process.

The mechanism proposed for the degradation of silicided graphite in air at 1550 °C will now be used to predict the effect of temperature on oxidation resistance. To this end, consider a temperature decrease of 200 °C (from 1550 °C to 1350 °C) and assume that in this temperature range the mechanism of silica growth according to reaction (5) does not change (at temperatures lower than 1350 °C, a change in the diffusion mechanism in the passive layer can occur[6]). The temperature-dependent variation in the growth rate of silica layer is calculated taking a value of 250 kJ/mol for the activation energy of the oxidation process.[6] With this value, the thickness of the passive layer at 1350 °C is found to be lower by a factor of 3 than its value at the reference temperature (1550 °C). For the same temperature change, the total pressure of SiO and CO species formed from reaction (2) for C-saturated SiC is reduced by a factor of 8. This factor would be even higher if, for kinetic reasons, the reaction (2) does not occur at equilibrium at 1350 °C. Therefore, at 1350 °C, the maximum of the $\Delta m/S$ vs time curve is expected to shift towards longer times, resulting in increasing lifetime. The effect of temperature predicted by our analysis is confirmed by the results obtained in [2] showing an increase in the lifetime of silicided graphite by a factor of 10 (from 20 h to 200 h) for a decrease in temperature of 200 °C. With regard to an increase in temperature above 1550 °C, the present analysis agrees with the intuitive idea that it will lead to decreasing lifetime. For instance, for an increase in temperature of 50 °C, the calculated value of e increases by 1.2 while the total pressure of SiO and CO species increases by a factor of 2.5, thus increasing considerably the driving force for bubble nucleation and growth. As seen in Table 3, when the oxidation temperature increases from 1550 °C to 1600 °C, the lifetime of SGI-graphite is reduced by one order of magnitude. This dramatical reduction of lifetime, observed for a relatively modest increase in temperature, underlines the double contribution of bubbles to the degradation of the silicided zone, consisting of the evacuation of reaction products from the reactive SiO_2/SiC interface and the direct exposure of graphite particles to oxygen.

5. Conclusions

Silicidation of graphite by RGI leads to the formation of a composite zone consisting of silicon carbide and graphite with, on its surface, a continuous SiC layer several tens of microns thick. The oxidation behaviour of silicided graphite in air at 1550 °C is dictated by two conflicting reactions: the passive oxidation of silica, which predominates at short times and results in a gain in material mass, and the reduction of the passive layer by the underlying silicon carbide, which predominates at longer times and causes mass losses. The lifetime of the material is strongly reduced by two factors inherent to the silicidation process, namely the unreacted carbon particles present in the continuous SiC layer, that enhance the reaction between silica and silicon carbide and cause bubble formation, and the presence on the material surface of sites of weak resistance to oxidation (consisting of places where the thickness of the continuous layer is much smaller than its average value) allowing the non-infiltrated porous graphite region to be attained rapidly by the oxidation front. The lifetime of graphite silicided by RGI was found as high as 74 h under air at 1550 °C but it decreased by one order of magnitude for a temperature increase of only 50 °C. This result clearly indicates that for this type of silicided graphite, the upper temperature limit is 1550 °C. According to the proposed analysis of the degradation process of the silicided zone in air, and in agreement with the experimental findings, the temporal stability of this zone and thus the material lifetime, increase rapidly with decreasing temperature. Graphite silicided by RLI resists to oxidation in air at 1550 °C quite well; however, due to a thinner continuous SiC layer, its lifetime is lower, by a factor of 1.6, compared to RGI-graphite.

Acknowledgements

The authors thank Dr C. Chatillon for the critical reading of the manuscript and helpful suggestions.

References

1. Einhaus R, Kraiem J, Drevet B, Cocco F, Enjalbert N, Dubois S, et al. Purifying UMG silicon at the French PHOTOSIL project. *Photovoltaics Int* 2010;(August):58–65.

2. Zhu Q, Qiu X, Ma C. Oxidation resistant SiC coating for graphite materials. *Carbon* 1999;**37**:1475–84.
3. Chunhe T, Jie G. Improvement in oxidation resistance of the nuclear graphite by reaction-coated SiC coating. *J Nucl Mater* 1995;**224**:103–8.
4. Zhu Y-C, Othani S, Sato Y, Iwamoto N. The improvement in oxidation resistance of CVD-SiC coated C/C composites by silicon infiltration pretreatment. *Carbon* 1998;**36**:929–35.
5. Paccaud O, Derré A. Reactive pack-cementation coating of silicon carbide on carbon-carbon composite. *J Phys IV France* 2001;**11**:1095–101.
6. Jacobson N. Corrosion of silicon-based ceramics in combustion environments. *J Am Ceram Soc* 1993;**76**:3–28.
7. Israel R, Voytovych R, Protsenko P, Drevet B, Camel D, Eustathopoulos N. Capillary interactions between molten silicon and porous graphite. *J Mater Sci* 2010;**45**:2210–7.
8. Eustathopoulos N, Israel R, Drevet B, Camel D. Reactive infiltration by Si: infiltration versus wetting. *Scr Mater* 2010;**62**:966–71.
9. Yun Y-H, Choi S-C, Chang J-C, Kim J-C. The conversion mechanism of SiC conversion layers on graphite substrates by CVR (Chemical Vapor Reaction). *J Ceram Proc Res* 2001;**2**:129–33.
10. Israel R. Etude des interactions entre silicium liquide et graphite pour application à l'élaboration du silicium photovoltaïque, Thesis, Polytechnique Institute of Grenoble, France; 2009, p. 95.
11. Touloukian YS, Kirby RK, Taylor RE, Lee TYR. Thermal expansion—nonmetallic solids. *Thermophys Properties of Matter*, 13. New York/Washington: IFI-Plenum; 1977.
12. Israel R. Etude des interactions entre silicium liquide et graphite pour application à l'élaboration du silicium photovoltaïque, Thesis, Polytechnique Institute of Grenoble, France; 2009, p. 166.
13. Paccaud O., Cémentation réactive de matériaux carbonés. Synthèse et caractérisation de revêtements de carbure de silicium, Thesis, Université Bordeaux I, France; 1994.
14. Paccaud O, Derré A. Silicon carbide coating by reactive pack-cementation – Part II: Silicon monoxide/carbon reaction. *Chem Vap Depos* 2000;**6**: 41–50.
15. Israel R. Etude des interactions entre silicium liquide et graphite pour application à l'élaboration du silicium photovoltaïque, Thesis, Polytechnique Institute of Grenoble, France; 2009, p. 86.
16. Israel R. Etude des interactions entre silicium liquide et graphite pour application à l'élaboration du silicium photovoltaïque, Thesis, Polytechnique Institute of Grenoble, France; 2009, p. 111.
17. Israel R. Etude des interactions entre silicium liquide et graphite pour application à l'élaboration du silicium photovoltaïque, Thesis, Polytechnique Institute of Grenoble, France; 2009, p. 120.
18. Heuer AH, Lou VLK. Volatility diagrams for silica, silicon nitride and silicon carbide and their application to high-temperature decomposition and oxidation. *J Am Ceram Soc* 1990;**74**:1540–3.
19. NIST-JANAF. *Thermochemical Tables, J. Phys. Chem. Ref. Data, Monograph No. 9*, 4th edn. New York: Am Chem Soc Am Inst Physics; 1998.
20. Incropera FP, Dewitt DP. *Fundamentals of heat and mass transfer*. 4th edn. John Wiley & Sons; 1996. p. 354, 374.
21. Mailliart O, Hodaj F, Chaumat V, Eustathopoulos N. Influence of oxygen partial pressure on the wetting of SiC by a Co–Si alloy. *Mater Sci Eng A* 2008;**495**:174–80.
22. Schneider B, Guette A, Naslain R, Cataldi M, Costecalde A. A theoretical and experimental approach to the active to passive transition in the oxidation of silicon carbide. *J Mater Sci* 1998;**33**:535–47.
23. Israel R. Etude des interactions entre silicium liquide et graphite pour application à l'élaboration du silicium photovoltaïque, Thesis, Polytechnique Institute of Grenoble, France; 2009, p. 137.
24. Goto T, Homma H, Hirai T. Effect of oxygen partial pressure on the high-temperature oxidation of CVD SiC. *Corros Sci* 2002;**44**:359–70.